

NIPER-444  
(DE90000222)

**USING IMAGE ANALYSIS TO DETERMINE PETROPHYSICAL  
PROPERTIES OF RESERVOIR ROCKS -- TOPICAL REPORT**

**By**  
**Liviu Tomutsa**  
**Alan Brinkmeyer**

**March 1990**

**Performed Under Cooperative Agreement No. FC22-83FE60149**

**IIT Research Institute**  
**National Institute for Petroleum and Energy Research**  
**Bartlesville, Oklahoma**



**Bartlesville Project Office**  
**U. S. DEPARTMENT OF ENERGY**  
**Bartlesville, Oklahoma**

**FOSSIL FUEL**

This report has been reproduced directly from the best available copy.

Available to DOE and DOE contractors from the Office Of Scientific and Technical Information, P.O. Box 62, Oak Ridge, TN 37831; prices available from (615)576-8401, FTS 626-8401.

Available to the public from the National Technical Information Service, U.S. Department of Commerce, 5285 Port Royal Rd., Springfield, VA 22161

Price: Printed     A03      
Microfiche A01

USING IMAGE ANALYSIS TO DETERMINE PETROPHYSICAL  
PROPERTIES OF RESERVOIR ROCKS

Topical Report

By  
Liviü Tomutsa  
Alan Brinkmeyer

March 1990

Work Performed Under Cooperative No. FC22-83FE60149

Prepared for  
U.S. Department of Energy  
Assistant Secretary for Fossil Energy

Robert Lemmon, Project Manager  
Bartlesville Project Office  
P.O. Box 1398  
Bartlesville, OK 74005

Prepared by  
IIT Research Institute  
National Institute for Petroleum and Energy Research  
P. O. Box 2128  
Bartlesville, OK 74005

## TABLE OF CONTENTS

	<u>Page</u>
Abstract .....	3
Introduction.....	3
Equipment.....	4
Hardware.....	4
Software .....	5
Permeability Measurements .....	7
Improvement in Permeability Prediction.....	7
Drill Cutting Measurements.....	13
Pore Size Measurements.....	13
Pore Throat Measurements.....	14
Pore Geometry.....	15
Fractal Studies.....	15
Grain Size.....	17
Grains and Pore Measurements.....	17
References.....	21

## TABLES

1. Measured versus calculated permeabilities.....	10
2. Comparison of core plug and simulated drill cuttings .....	11
3. Grain measurements.....	15

## ILLUSTRATIONS

1. Thin section image before (A) and after (B) enhancement by histogram expansion.....	6
2. Pixel intensity histogram of the original image and the enhanced image.....	6
3. Porosity and specific surface vs. the number of dilations/erosions.....	9
4. Predicted permeability vs. the number of dilations/erosions.....	10
5. Permeability (millidarcy) across thin section P14454.5 .....	11
6. Pore size distributions for two typical rock types from barrier bar deposit.....	14
7. Pore throat distribution for thin section P1 - 4454.5.....	15
8. The number of perimeter pixels (N) vs. the pixel size (L) for a sandstone sample.....	16

# USING IMAGE ANALYSIS TO DETERMINE PETROPHYSICAL PROPERTIES OF RESERVOIR ROCKS

by

Liviu Tomutsa and Alan Brinkmeyer

---

## ABSTRACT

The objective of this work is to apply computer image analysis methods to measurements of pore and grain parameters in reservoir rocks and to use the measured values of these parameters to predict petrophysical properties such as porosity, permeability, and capillary pressure. By computer image analysis, rapid measurements of pore and grain diameters, areas, and perimeters can be performed, and from these measurements various other parameters, such as shape factor, form factor, and specific surface can be derived.

A commercially available PC-based image analysis system previously adapted for computations of petrophysical properties has been improved. Based on pore and pore throat measurements, rapid and reliable predictions of porosity, permeability, grain size distribution, and capillary pressure can be made from thin sections fabricated from rock samples as small as drill cuttings.

This report represents the completion of milestone 5 of the FY89 plan for Project BE12A and covers the work performed during FY89.

## INTRODUCTION

Oil and gas recovery can be performed in an efficient manner only by understanding rock structure, fluids and rock-fluid interactions in reservoirs. Pore space characteristics strongly influence entrapment of oil, gas storage, and fluid flow within reservoirs. Traditionally, pore throat information has been obtained either directly from optical or scanning electron microscopy of thin sections, polished slabs, or pore casts, or indirectly from mercury injection or centrifuge capillary pressure measurements performed on core plugs. Recent advances in computer image analysis hardware and software have provided new tools to help increase the accuracy and reduce the time of petrographic image analysis. Pore and grain quantitative data can be generated from microscopic images to determine important petrophysical properties such as porosity, permeability, and capillary pressure. This approach is especially useful whenever only small amounts of rock material such as drill cuttings or side wall plugs are available.

Work performed at NIPER in this area has involved setting up a computer image analysis system for petrographic studies and improving the methodology for generating good contrast images to be used in this system.<sup>1</sup>

Once good quality pore images are available, various methods from regression analysis<sup>2</sup> to flow models<sup>3</sup> can be used to predict petrophysical values for the rocks sampled. When the pore network of the rock satisfies the criteria in the Kozeny-Carman model flow in porous media,<sup>4</sup> rapid and accurate calculations of permeability based on image analysis data are possible.

## **EQUIPMENT**

### **Hardware**

The system,<sup>1</sup> consists of a light microscope with a fluorescent light attachment, a low-light black and white camera for fluorescent light work, a color camera for transmitted light work, image-capture and processing hardware and software, and a PC-AT compatible microcomputer.

Improvements in the system have increased operator efficiency and the capacity to store and process a large number of images in batch mode without operator intervention, thus taking full advantage of the system's programming language.

Modifications made to improve the system's parfocality have made comparison of captured images visible on the system monitor to direct images visible through a microscope eyepiece much easier. A three-megabyte RAM disk was added to the computer for increased speed in image manipulations.

A 40-megabyte backup tape cartridge drive was installed to allow efficient and economical storage of image files. This addition allows testing various software algorithms on the same image. Unless test images are stored in digitized files, it is difficult and time-consuming to recapture the images everytime they are needed by resetting exactly the same microscope adjustments.

By adding a higher resolution color camera, the resolution of the camera output matches more closely the resolution of the image capture board; thus, the quality of color images obtained in the transmitted light mode has been improved.

For the micrometer or submicrometer range, such as pore throats or pore surface geometry, images generated by an optical microscope do not have the required resolution and must be replaced

by images generated by a scanning electron microscope (SEM). Two approaches are possible in transferring SEM images to the image analysis computer:

(1) direct transfer of the slow-scan SEM image to the image capture board. This feature is available only on late model SEMs which provide a pixel clock signal for proper pixel alignment in image transfer;

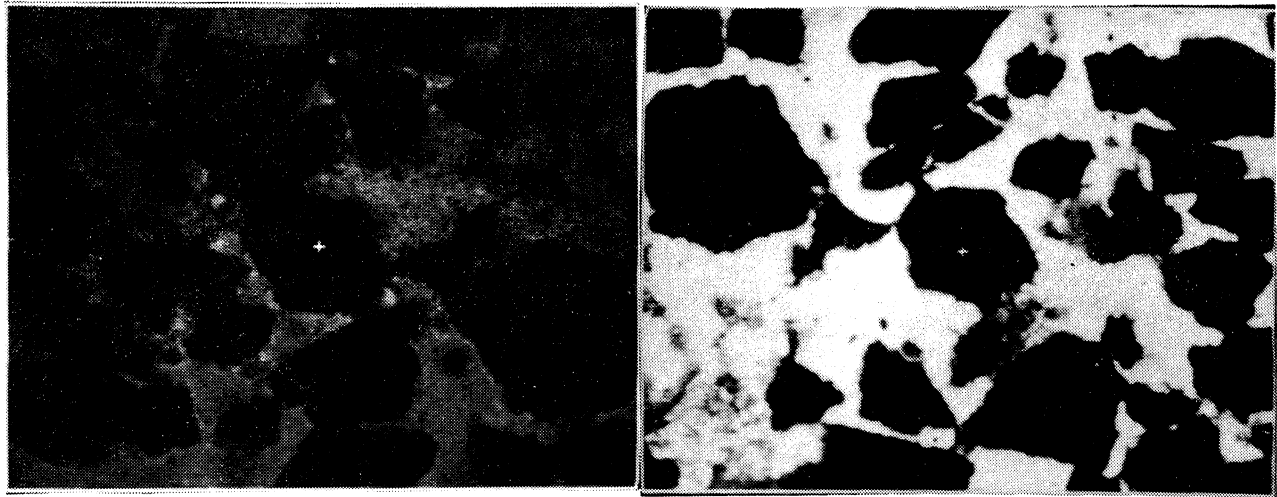
(2) high-resolution photography (either Polaroid or 35 mm) of SEM images and capture of the photographed image by means of a high-resolution black and white camera. This is the necessary approach with older instruments which do not provide a pixel clock signal. This approach of image transfer yields no information loss providing that the SEM photograph and the video equipment have a higher resolution than the image analysis equipment, the video camera has a high signal-to-noise ratio, and high quality optics are used.

In the experimental setup, SEM images are photographed on Polaroid film and then transferred into the computer by using a high-resolution Dage-MTI™ camera. The backscatter electron images obtained from the SEM provide very good resolution of pore from nonpore features for magnifications greater than 40X. Images obtained with 46X magnification are at a scale approximately equal to those obtained with the optical microscope and a 5X objective. The highest magnification used for these investigations was 300X because of the limited number of pores covered by the magnified image.

### **Software**

Four improvements made in the image-handling and analysis software increased the overall system efficiency. The program listings are available upon request directly from the authors.

Histogram plotting and expansion algorithms allow for plotting histograms of gray levels for image pixels to change their value for increased image contrast and to replot histograms for an optimum threshold selector. Histogram expansion is performed in two steps. First, the histogram is shifted to the left-hand side so the lowest pixel value becomes zero, then the histogram is stretched so the highest pixel value becomes 255. The left-hand shift is performed by subtracting a constant from all image pixel values, and the stretching, by multiplying all pixels by a second constant. Improvement in image contrast using the histogram expansion software is shown in figure 1. It can be seen that more detail is shown by the enhanced image. Figure 2 is a pixel intensity histogram of both the original and improved image using the histogram expansion.



(A)

(B)

FIGURE 1. - Thin section image before (A) and after (B) enhancement by histogram expansion.

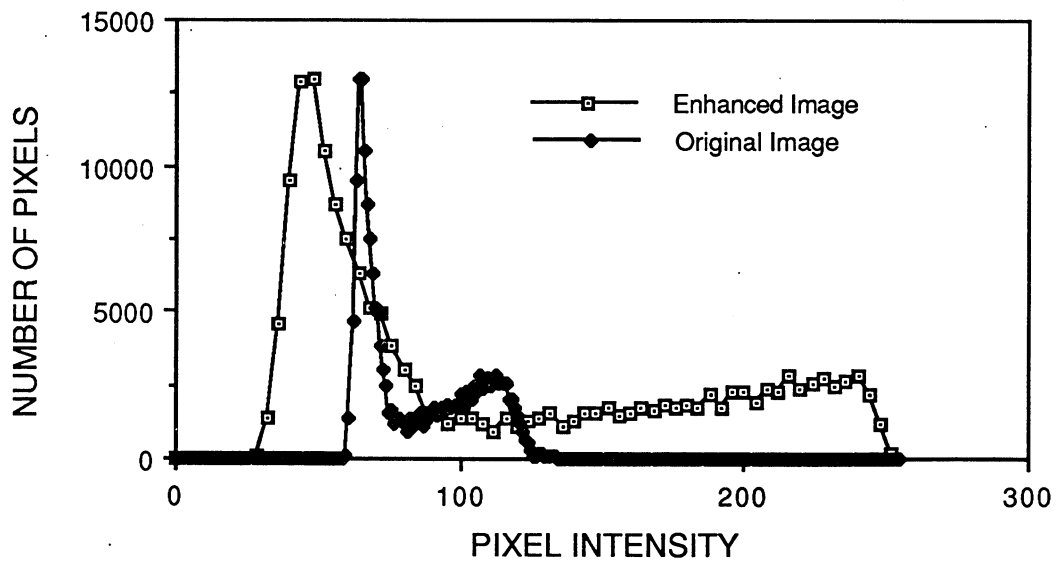


FIGURE 2. - Pixel intensity histogram of an original image and an enhanced image.

When histogram expansion is used, gray level values are changed, and the gray-level threshold must be adjusted to new values to define the pore/grain interface correctly.

The image file compression algorithm reduces the data file from 0.6 to 0.2 megabyte allowing better usage of both RAM and disk and tape storage. Each image file has a format by which each screen pixel is represented by three bytes of computer memory. The screen resolution being 512 x 400 pixels translates into storage requirements for 512 x 400 x 3, or 614,400 bytes. These three bytes represent the hue, saturation, and luma values of each pixel. Black and white images, by definition, are made up of pixels with varying gray levels only; that is constant hue and saturation and varying luma. Therefore the only values necessary to represent a black and white image are those values represented by the luma byte of each pixel, thereby reducing the file size by a factor of three. The reduced files are then stored on a 40-megabyte removable tape cartridge. When needed, the original image file can be reconstructed by adding the hue and saturation channels.

The image averaging algorithm allows averaging of noisy, low contrast images for improving image quality.

The pseudocoloring algorithm attaches operator-selected colors to various gray level ranges present in the original image. Because the eye can resolve colors easier than gray levels, the false color image can help in certain cases in resolving features which would be difficult to resolve in black and white.

## **PERMEABILITY MEASUREMENTS**

### **Improvement In Permeability Prediction**

Because of the type of rock studied, clean sandstone of relatively large permeability and porosity, the Kozeny-Carman model was selected for predictions of permeability based on pore measurements performed on thin sections by image analysis.

The Kozeny-Carman equation for permeability is defined:

$$k_{ck} = \frac{\phi^3}{k_c S_o^2 (1-\phi)^2} \quad (1)$$

where:

$k_{ck}$  = permeability (md)

$\phi$  = porosity

$k_c$  = Kozeny constant

$$S_o = \left(\frac{4}{\pi}\right) \left(\frac{\text{pore perimeter}}{\text{pore area}}\right) = \text{specific surface}$$

In its derivation, equation 1 assumes pores with "smooth" walls. The porous media were modeled as a conduit of a hydraulic diameter,  $D$ , defined by:

$$D = \frac{4\phi}{S_o (1-\phi)} \quad (2)$$

For certain large pores with very rough surfaces or for images with poor pore-nonpore contrast,  $S_o$  could be excessively large if the initial large raw value for the measured perimeter is used in calculating  $S_o$ . This, in turn, could yield an erroneously small  $D$  value and an erroneously small value for the computed Kozeny-Carman permeability. The "smooth" component of the perimeter to be used in calculating a correct  $S_o$  can be obtained (a) by selecting the proper microscope magnification such that the pixel size is greater than the size of irregularities, and (b) by applying dilations and erosions on the original image.

An image-processing algorithm for "smoothing" pore perimeters has been applied to several SEM-BEI generated images and color images obtained from transmitted light. The algorithm consists of applying successive image-processing dilations and erosions on the pore image, measuring the porosity and specific surface, and computing  $k_{ck}$ . The dilation procedure adds one pixel to the exterior of each feature, while the erosion removes a pixel from the exterior of each feature. The dilation-erosion procedure results in a relatively constant total area of a feature. However, dilation-erosion reduces surface roughness and decreases the feature perimeter and the specific surface.

Thus, the value of the specific surface decreases by increasing the number of dilation-erosion operations until a relatively stable value is obtained, as shown in figure 3.

Permeability estimates were made for images from thin sections based on the Kozeny-Carman equation. The effect of reducing the surface roughness was tested by increasing the number of dilation-erosion operations and calculating the permeability,  $k_{ck}$ . For the example shown in figure 4,  $k_{ck}$  increased from 900 to a maximum of 2,300 md. The measured permeability of this core sample was 2,077 md. The dilation-erosion operation appears to improve the agreement between measured and computed permeability values. Although the optimum number of dilation-erosion operations varies from case to case, the use of two dilations followed by two erosions provides an adequate "smoothing" of the pore perimeter without significantly changing the original shape of the pore geometry.

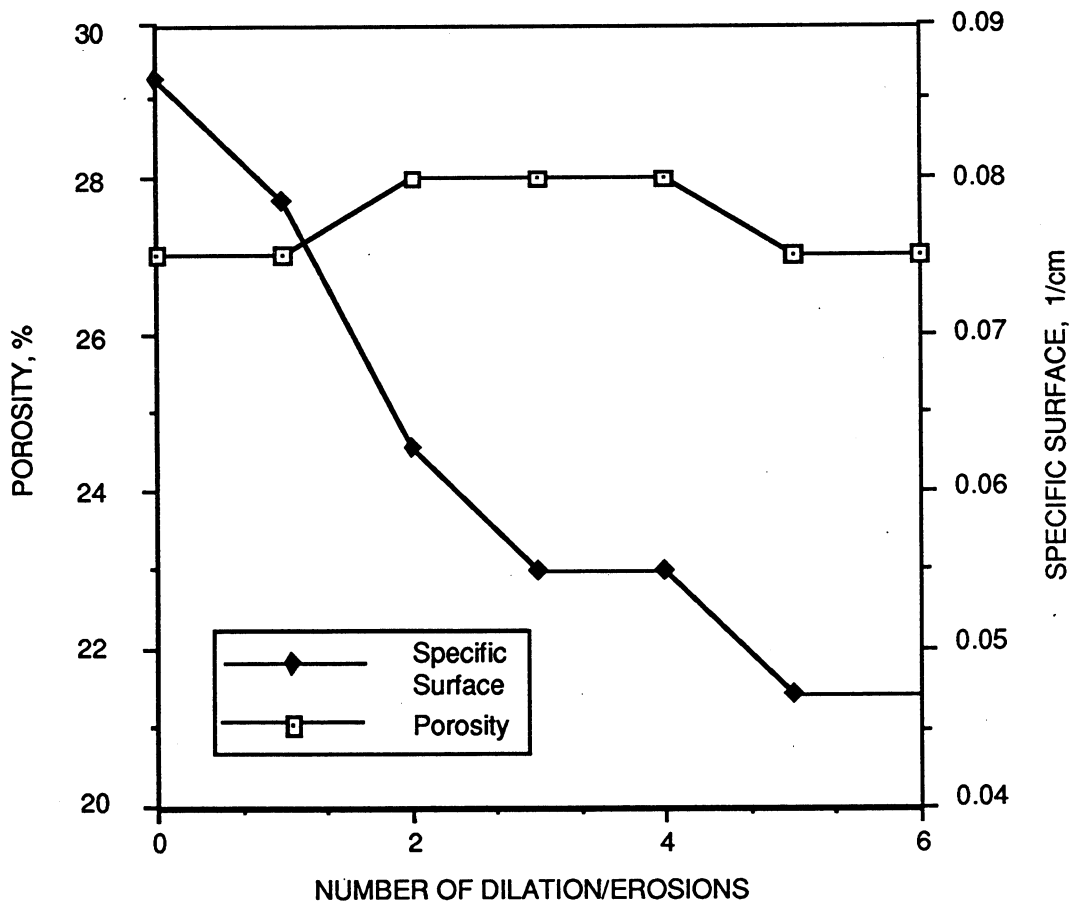


FIGURE 3. - Porosity and specific surface vs. the number of dilations/erosions.

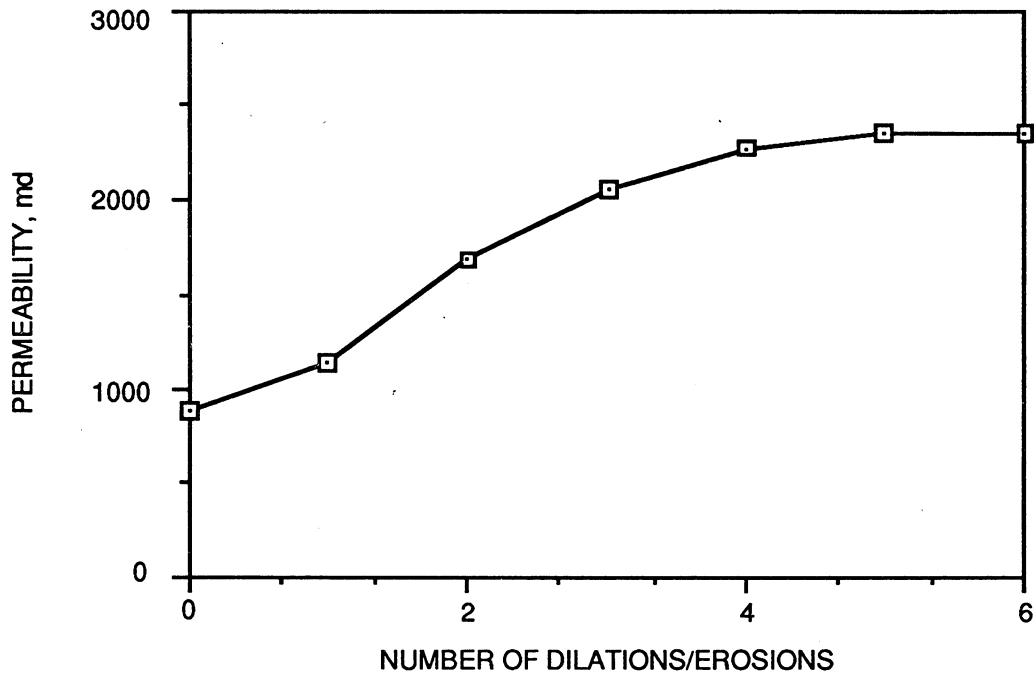


FIGURE 4. - Predicted permeability vs. the number of dilations/erosions.

With two dilations-erosions, 30 images from a thin section can be processed in about 2 hours and a permeability value generated.

When significant variations of pore structure are observed across a thin section, the arithmetic average of the permeability for the images across the thin section may not equal the plug value. The Kozeny-Carman permeabilities at 20 locations across such a thin section and the isoperm contours are shown in figure 5. A trend of increasing permeabilities from the upper right-hand corner toward the lower left-hand corner can be observed. To use thin section-computed permeabilities to calculate a core plug permeability, how the two-dimensional (2D) trend observed in the thin section is related to the (3D) three-dimensional pore distribution trend in the core plug must be known. In the absence of such information, the range of expected Kozeny-Carman permeability for the thin section can be determined by calculating the arithmetic, geometric, and harmonic averages of the Kozeny-Carman permeabilities based on the values obtained for the individual images processed for each thin section.

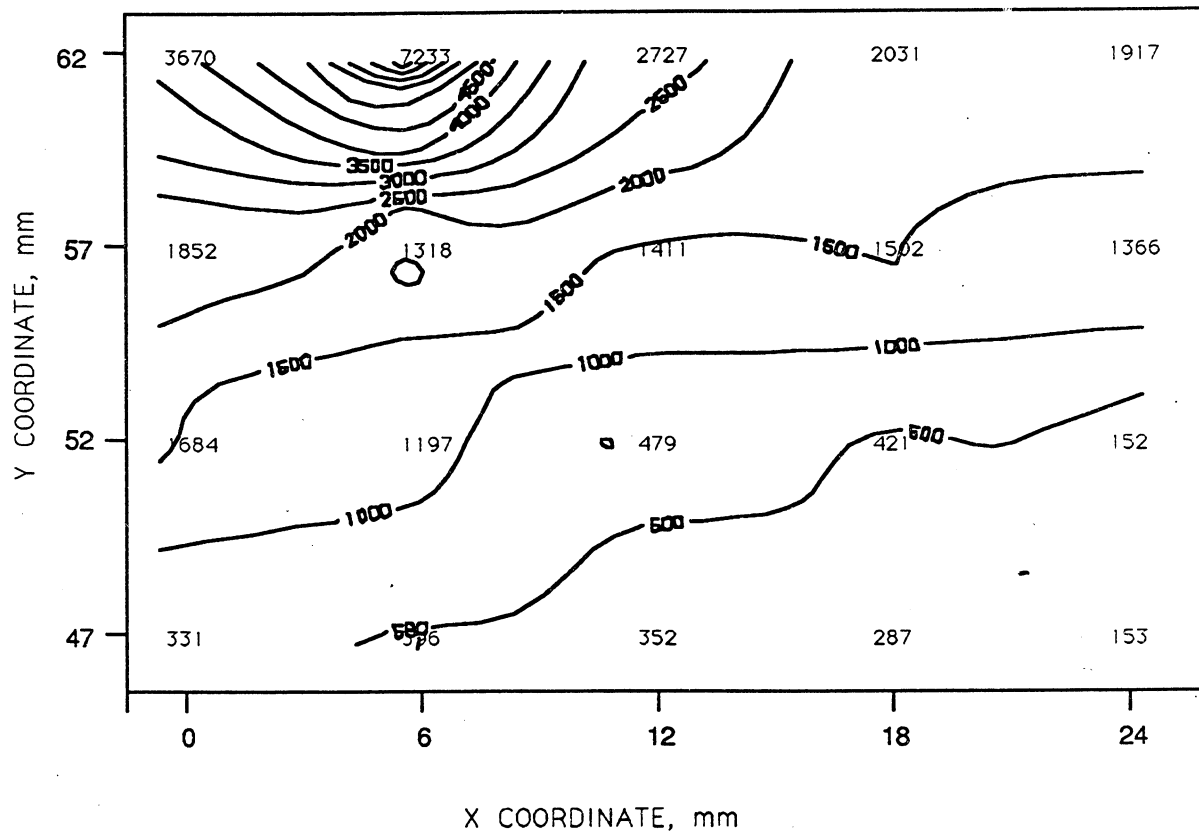


FIGURE 5. - Permeability (millidarcy) across thin section P14454.5, millidarcies.

The Kozeny-Carman permeabilities calculated are compared to the plug permeabilities in table 1 by using both fluorescent and transmitted light images. Discrepancies between plug and thin section permeabilities are due to the clay-caused heterogeneity. The comments in the last column of table 1 are based on direct observations in transmitted light. Because of the low contrast difference between the clay-filled and the empty pore space, under fluorescent light, values for image-generated porosity and permeability which are larger than the corresponding plug values are often obtained.

For thin sections with low clay content, a correct value of permeability can be determined by using fluorescent light. If a bulk porosity value is available for a thin section, it can be used in the selection of the image segmentation threshold for improved permeability calculations. The image segmentation threshold for which the thin section porosity will be equal to the plug porosity is selected, and binary images obtained with such threshold are used to calculate the permeability.

For thin sections with large clay content where significant microporosities are present, images obtained from either transmitted light or scanning electron microscope backscattered electrons, should be used.

TABLE 1. - Measured versus calculated permeabilities

Well	Depth, ft	k Plug, md	kck, <sup>1</sup> md	Comments
C4	4,340.2	53	166	Abundant clay, pore throats plugged.
C4	4,342.6	447	430	Clay cement, clay laminae.
C4	4,344.6	212	194	Clay cement, clay laminae.
C4	4,346.4	896	779	Uniformly distributed clay.
C4	4,350.6	1,645	1,209	-
C4	4,351.6	428	345	Uniformly distributed clay. Discrete clumps.
C4	4,357.1	1,094	1,119	Uniformly distributed clay.
P1	4,442.1	667	665	-
P1	4,447.8	1,446	1,524	Undercompacted grains.
P1	4,454.5	1,150	1,411	Clay rims around grains. Throats affected.
P1	4,456.8	911	1,426	Clay laminae.
W7	4,415.5	0.67	<sup>2</sup> (0.14)	Poorly sorted: Clay in pore throats.
W7	4,417.5	52	90	Very poorly sorted. Large clay amount in throats.
W7	4,419.5	1,730	1,003	Clay laminae alternate with very porous layers.
W7	4,423.8	1,024	1,026	Clean sample.
W7	3,318.4	279	543	Clay rims. Clay in pore throats.

<sup>1</sup>Kozeny-Carman permeability.

<sup>2</sup>Using color image.

### Drill Cutting Measurements

Drill cuttings of a few millimeters in diameter were prepared from two Berea sandstone core plugs of measured porosities and permeabilities (19.8%, 192 md, and 19.2%, 82 md, respectively) and were used in making thin sections.

A very good agreement was obtained between the permeability calculated by image analysis from the thin section and the core plug values. The good agreement resulted from the clean rock in the samples.

Several procedures were used in studies to measure the porosity of drill cuttings. Simulated drill cuttings were made by crushing rock samples and sized by sieving (8 to 12 mesh and 6 to 8 mesh). The procedures included liquid saturation (mineral oil) of drill cuttings and liquid displacement in a pycnometer to obtain pore and bulk volumes. These procedures did not produce porosity values with sufficient accuracy. Another procedure involved mercury displacement by drill cuttings to obtain bulk volume of a drill cutting sample. This method resulted in too high bulk volumes because of air trapped in the sample container and between drill cuttings. This, in turn, yielded too large porosity values.

The final procedure involved measuring the grain volume of a 7 to 9 grain drill cutting sample by using Boyle's law. The sample was then placed in a syringe and the syringe filled with an excess of mercury to completely immerse the drill cuttings. Most of the trapped air was then expelled from the syringe and the syringe needle sealed with a rubber stopper. Mercury was then injected into the remaining air trapped between drill cuttings by increasing pressure on the syringe barrel. The weight and volumes were then compared with the syringe completely filled with mercury to obtain the sample bulk volume. Some of the results obtained by this procedure are compared with porosity values measured from core plugs in table 2. It appears that, with further refinements, porosity values of necessary accuracy for image analysis calibration can be measured by this technique for drill cuttings from well consolidated cores.

TABLE 2. - Comparison of core plug and simulated drill cutting porosity

Core sample	Plug porosity, %	Mesh	Drill cutting porosity, %
B1	20	8-12	21.5
B2	25	8-12	28
L1	12	8-12	13
B5	25	6-8	22
B6	17.7	6-8	19
L2	11.3	6-8	10.5

### Pore Size Measurements

To test the correlation between the pore size distribution measured by image analysis and both plug permeability and thin section completed permeability, pore sizes were measured for various thin sections representing different rock types of a barrier bar deposit (fig. 6). Only the pores with diameters larger than 6  $\mu\text{m}$  were considered for these distributions to avoid counting small artifacts (few pixels in size) due to noise in the images. The feature size distribution can have fractal behavior, with large numbers of small features contributing much less to the total optical porosity than the fewer in number but larger features. The small features, while contributing very little to porosity (less than 1%), can lower the Kozeny-Carman permeability to less than half the plug value. The high-permeability sample had a larger fraction of large pores than the low-permeability sample, as expected.

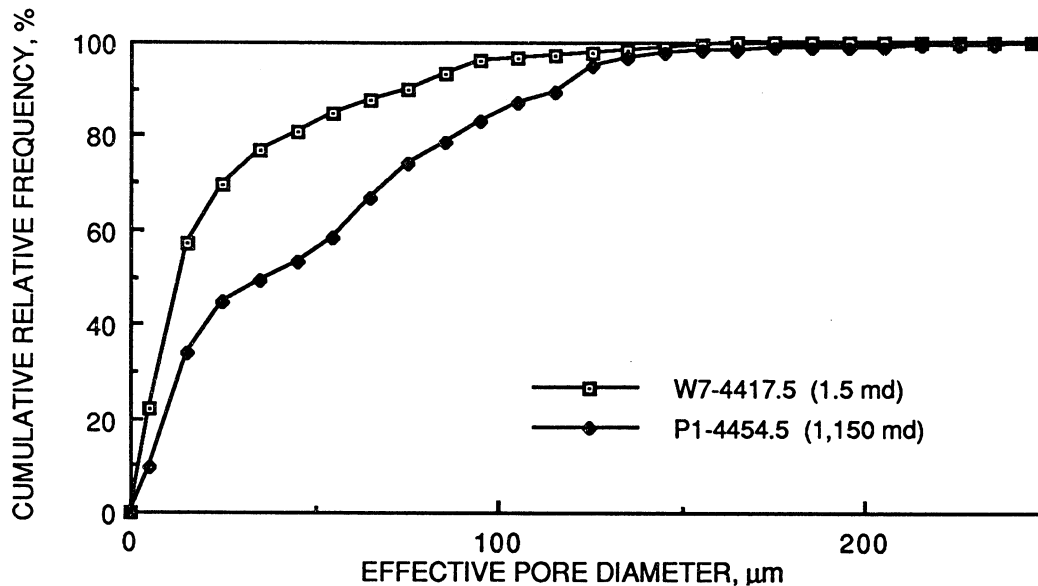


FIGURE 6. - Pore size distributions for two typical rock types from a barrier bar deposit.

### Pore Throat Measurements

A mercury injection apparatus was improved by adding digital gauges and an accurate pump. The system provides accurate measurements of pore throats from 100 to 0.1  $\mu\text{m}$ , which is the range of interest for rock investigations by image analysis.

Mercury was injected into 15 cores taken from various facies of a barrier bar deposit. Pore throat distributions measured by mercury injection and image analysis (40 X objective) are shown in

figure 7. Good agreement between the two measurements is shown for throats larger than 4  $\mu\text{m}$ , which is near the resolution limit of the optical microscope.

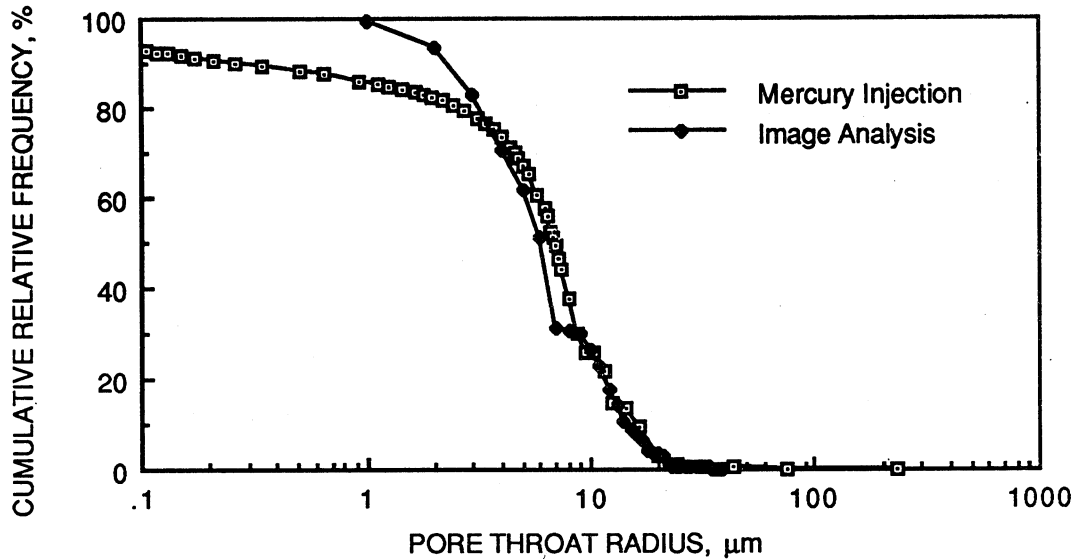


FIGURE 7 - Pore throat distribution for thin section P1 - 4454.5.

## PORE GEOMETRY

### Fractal Studies

The geometry of many irregular shapes encountered in nature from clouds, landscapes, and coastlines to rock grains, fluid flow lines, and particle aggregates can be described by the new mathematical theory of "fractals" developed by Mandelbrot.<sup>6</sup> The subject of this theory is the study of irregular shapes mentioned above plus other "pathological" mathematical objects which do not fit in classical geometry. Their main characteristic is that in some way their shapes show similarities of various scales of observation, or that the fractal objects are made up of parts similar in some way to the whole.

A good review of the application of fractal theory to fluid flow in porous media has been given by Feder.<sup>7</sup> Krohn and Thompson<sup>8</sup> have measured the fractal dimension of the pore/rock interface. Hewett and Behrens<sup>9</sup> have used fractal properties of reservoir heterogeneities to improve the accuracy of reservoir simulations. The computation of fractal dimensions of pore surface volume is a necessary step toward an accurate description and modeling of porous medium. To be able to

perform this computation, measurements of pore geometry have to be performed at various scales of detail by changing the size of the measuring unit. This can be performed either by changing the magnification of the image and using the screen pixel calibration to the respective scale or by using the image with the largest magnification and varying the size of the pixels used for measurements.

Given the level of detail needed, SEM BEI images have to be used. By using such images at magnifications of 300X, 250X, 200X, 150X, 100X, and 50X and measuring the pore perimeter, the fractal dimension of the pore/rock boundary perimeter for one thin section has been calculated to be 1.63, which is within the range quoted in the literature for sandstone rocks (fig. 8). The number of pixels (N) contacting the perimeter is related to the pixel size (L) by the formula:  $N = aL^{-D}$  where  $a = 3.27$ ,  $D = 1.632$ ,  $r^2 = 0.99$ . The fractal dimension is the slope of the linear regression  $\log(N)$  vs  $\log(L)$ .

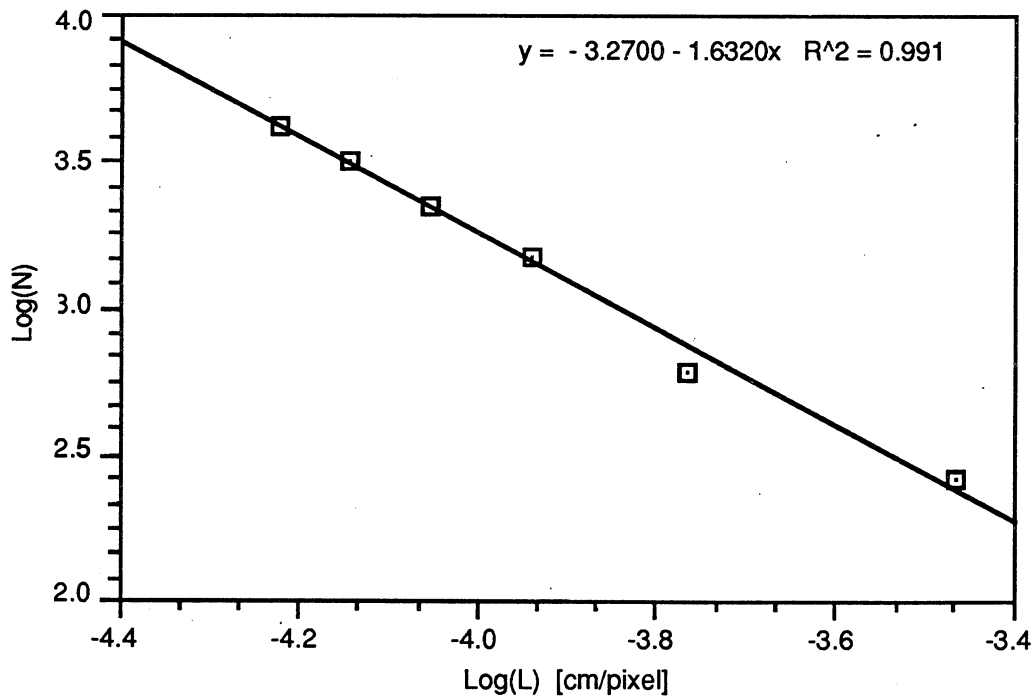


FIGURE 8. - The number of perimeter pixels (N) vs. the pixel size (L) for a sandstone sample.

## GRAIN SIZE

### Grains and Pore Measurements

Measurements of grains and pores were made on thin sections representing various facies of a barrier bar reservoir by both image analysis and point count. The thin sections measured represent a

good variety of pore and grain size and clay content. A good understanding is also available for the depositional and diagenetic environment at these locations. Arithmetic averages and standard deviations for major and minor grain diameters are shown in table 3.

TABLE 3. - Grain measurements

Well	Depth, ft	Permeability, md	Porosity, %	Rock type <sup>1</sup>	Majd, <sup>2</sup> μm	Majst, <sup>3</sup> μm	Mind, <sup>4</sup> μm	Minst, <sup>5</sup> μm
C4	4340.2	53.00	24.6	1	105	41	63	27
C4	4342.6	447.00	27.8	1	119	49	69	30
C4	4344.6	212.00	22.8	2	112	41	63	26
C4	4346.4	896.00	27.1	2	99	31	63	21
C4	4350.6	1645.00	28.0	2	143	44	92	33
C4	4357.1	1094.00	28.8	2	134	43	79	27
P1	4438.6	0.93	8.0	1	87	55	51	31
P1	4442.4	667.00	31.0	2	141	52	82	32
P1	4447.8	1446.00	31.0	2	145	49	81	28
P1	4449.5	720.00	31.4	2	144	57	87	37
P1	4454.5	1150.00	32.1	2	135	52	78	35
P1	4456.8	911.00	32.2	2	129	37	77	24
P1	4458.7	2.80	10.0	3	62	33	38	22
P1	4459.0	9.50	13.9	3	51	21	32	13
P2	4413.5	298.00	25.5	1	127	61	80	39
P2	4414.3	61.00	26.8	1	73	48	43	25
P2	4417.2	2546.00	27.6	2	123	71	75	43
P2	4418.5	2414.00	28.6	2	123	67	74	42
P2	4421.5	3994.00	29.0	2	112	65	68	40
P2	4423.5	3186.00	29.6	2	117	68	69	41
P2	4425.5	2438.00	29.4	2	114	53	69	32
P2	4430.5	3337.00	29.3	2	113	68	66	40
P2	4433.2	2747.00	29.9	2	85	64	50	35
P2	4437.1	186.00	22.5	3	67	48	43	30
P2	4438.3	1.00	15.0	3	27	22	17	12
W7	4415.5	0.67	15.3	1	90	50	52	31
W7	4417.5	52.00	19.7	1	101	53	56	33
W7	4419.5	1730.00	28.7	2	106	35	60	22
W7	4421.8	207.00	27.4	2	98	35	58	20
W7	4427.5	1503.00	28.7	2	107	46	64	29
W7	4428.5	279.00	25.9	2	117	45	69	31
W7	4431.3	433.00	30.2	2	134	54	76	33
W10	4354.5	1.00	15.0	3	64	44	41	25

<sup>1</sup>Rock

1 = Lagoon and valley fill.

2 = Middle, foreshore, upper shoreface, and beach.

3 = Lower shoreface.

<sup>2</sup>Majd = major diameter of grain.

<sup>3</sup>Majst = major diameter standard deviation.

<sup>4</sup>Mind = minimum diameter of grain.

<sup>5</sup>Minst = minimum standard deviation.

Both the log of permeability and the porosity correlate relatively well to the major grain diameter ( $r^2 = 0.7$ ) shown in figures 9 and 10.

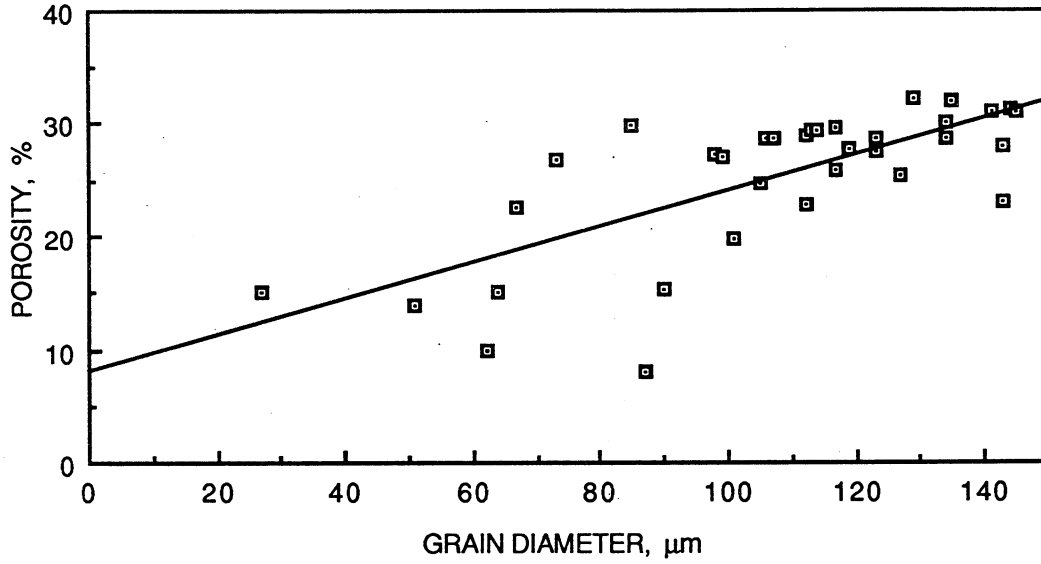


FIGURE 9. - Core plug permeability vs. average grain major diameter.

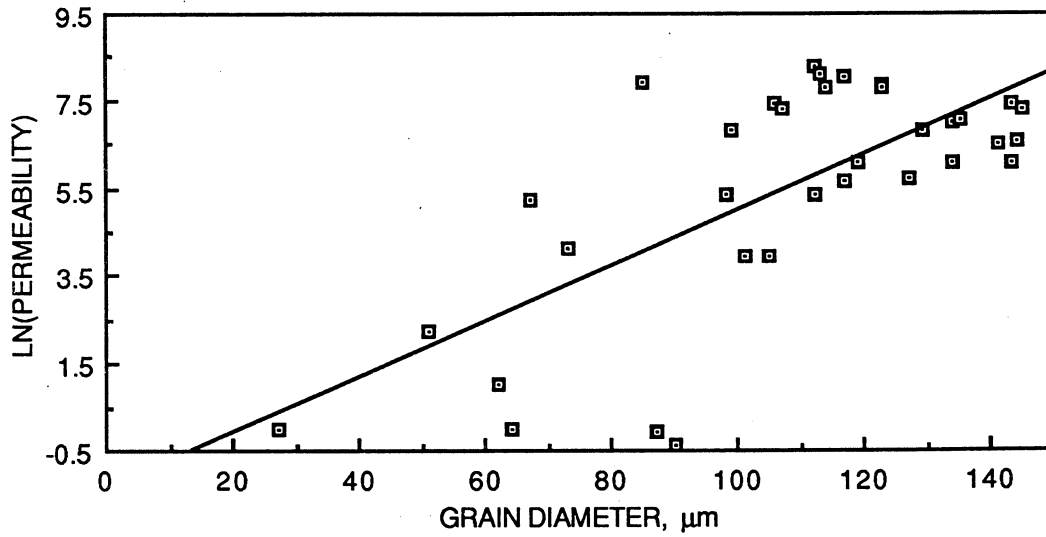


FIGURE 10. - Core plug porosity vs. average grain major diameter.

A comparison between grain diameters obtained by computer image analysis and manual point counting indicates good correlation ( $r^2 = 0.79$ ) (fig. 11). Note that the two methods yield different actual values for grain size averages because of differences in the basic procedures of each method. The image analysis method was used here on fluorescent images. The fluorescent image captures only features on the surface of the thin section while the transmitted light views a cross section of the thin section. Therefore the fluorescent image will generate smaller grain sizes than the transmitted light. Also, the features measured by image analysis were not only complete quartz grains but also grain fragments and possibly small matrix clumps or areas of cement, which had the same gray level as the grains. The manual point count method used transmitted light in which only quartz grains from the original depositional process were counted on only 200 points. For small grains ( $<100 \mu\text{m}$ ), more than 400 or more points should be counted.

After the calibration curve is established by using a small number of point-counted thin sections and image analysis on fluorescent images, significant time savings can be achieved in measuring the average quartz grain size by using only the image analysis method.

By using the image analysis system with a color camera and performing individual quartz grain measurements using a screen cursor, a close agreement can be obtained between the image analysis and the numerical point count. While this approach has the advantage of eliminating the need for

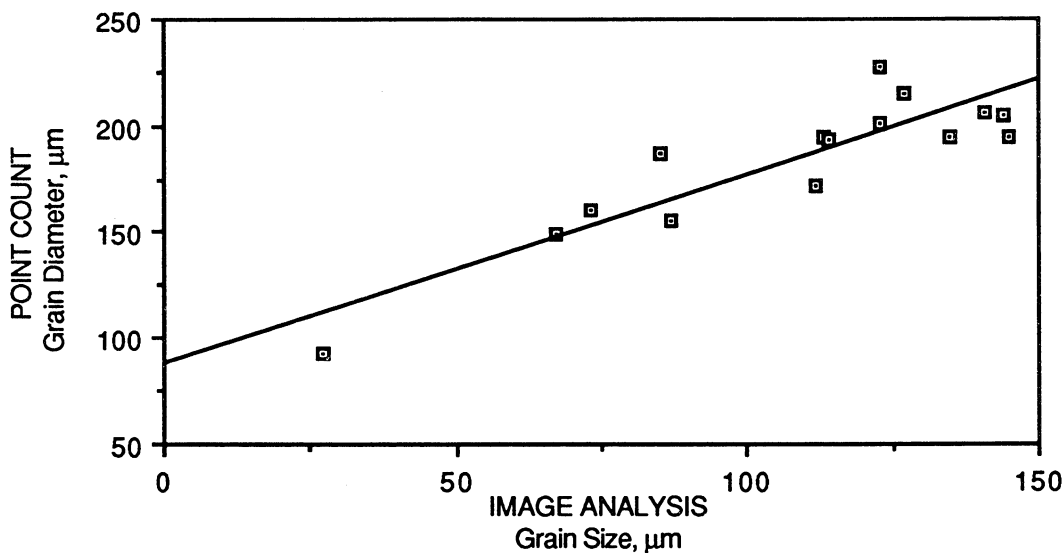


FIGURE 11. - Correlation of point count and image analysis measurements.

a calibration curve, it is slower than automatic measurements performed on fluorescent images. Nevertheless, it is faster by a factor of two or three over a manual point count.

The comparison between these two grain size measurement methods shows the importance of specifying essential details of the measurement procedure together with actual measurement results. This allows the user of the measurement results to evaluate correct range applicability.

## REFERENCES

1. Tomutsa, L., Alan Brinkmeyer, and Clarence Raible. Determining Petrophysical Properties of Reservoir Rocks by Image Analysis. Department of Energy Report No. NIPER-378, October 1988. NTIS order No. DE89000734.
2. Elrich, R., K. O. Horkowitz, T. P. Horkowitz, and S. J. Crabtree Jr. Objective and Functional Classification of Reservoir Porosity: Relating PIA to Petrophysics. AAPG Bull. Feb. 12, 1987.
3. Dullien, F. A. L. Porous Media, Fluid Transport and Pore Structure. Academic Press, Inc., New York, 1979.
4. Berryman, J. G. and S. C. Blair. Use of Digital Image Analysis to Estimate Fluid Permeability of Porous Materials: Application to Two-Point Correlation Functions. J. Appl. Phys., v. 60, 1986, p. 1930.
5. Bush, C. D. and D. L. Freeman. Drill Cuttings Porosity Grain Density and Permeability by Direct Laboratory Measurements and Their Reliability. Pres. at SPWLA 27th Annual Logging Symp., June 9-13, 1986.
6. Mandelbrot, B. B. The Fractal Geometry of Nature. Freeman, New York, 1982.
7. Feder, J. Fractals. Plenum Publishing Company, New York, 1988.
8. Krohn, C. E. and A. H. Thompson. Fractal Sandstone Pores: Automated Measurements Using Scanning-Electron-Microscope Images. Phys. Rev. B., v. 33, 1986, p. 6366.
9. Hewett, T. A. and R. A. Behrens. Conditions Simulation of Reservoir Heterogeneity with Fractals. Pres. at the SPE Ann. Tech. Conf. and Exhib., Houston, TX, Oct. 2-5, 1988. SPE paper 18326.



